THE CHANDRA X-RAY OBSERVATORY

Martin C. Weisskopf
Space Sciences Department
NASA/Marshall Space Flight Center, AL 35812

ABSTRACT

The Chandra X-Ray Observatory is the X-ray component of NASA's Great Observatory Program. The facility provides scientific data to the international astronomical community in response to peer-reviewed proposals for its use. Data becomes public at most one year after the observation. The Observatory is the result of the efforts of many academic, commercial, and government organizations in the United States and Europe. NASA's Marshall Space Flight Center (MSFC) manages the Project and provides Project Science; NGST (formerly TRW) served as prime contractor responsible for providing the spacecraft, the telescope, and assembling and testing the Observatory; and the Smithsonian Astrophysical Observatory (SAO) provides technical support and is responsible for ground operations including the Chandra X-Ray Center (CXC). We present a description of the hardware and an overview of some of the remarkable discoveries.

Figure 1: Professor Subramanyan Chandrasekhar.

1 The Observatory

In 1977, NASA/MSFC and SAO began a study which led to the definition of the then named Advanced X-Ray Astrophysics Facility. This study had been initiated as a result of an unsolicited proposal submitted to NASA in 1976 by Prof. R. Giacconi (Harvard University and SAO) and Dr. H. Tananbaum (SAO). Many significant events took place during the intervening years including the highest recommendation by the National Academy of Sciences Astronomy Survey Committee in the report, "Astronomy and Astrophysics for the 1980's"; selection of the instruments in 1985; selection of the prime contractor in 1988; demonstration of the ability to build the flight optics in 1991; restructuring the mission to reduce cost, primarily by eliminating servicing, in 1992; selecting the name of the mission in honor of the Nobel Prize winner Subramanyan Chandrasekhar in 1998 (Figure 1); and the launch the following year. This past year, Prof. Giacconi (Figure 2) was awarded the Nobel Prize for his pioneering work in X-ray astronomy.

The launch took place on July 23, 1999 using the Space Shuttle Columbia. The Commander was Col. Eileen Collins (Figure 3), the first female commander

Figure 2: Professor Riccardo Giacconi.

of a Shuttle flight. The rest of the crew were: Jeffrey Ashby the pilot; and mission specialists Catherine Cady Coleman, Steven Hawley, and Michel Tognini. With a second rocket system, the Inertial Upper Stage (IUS) attached, the Observatory was both the largest and the heaviest payload ever launched by, and deployed from, a Space Shuttle. Figure 4 shows the IUS mated to the Observatory and both mounted in Columbia's cargo bay just prior to launch.

Once deployed, and after separating from the IUS, the flight system illustrated in Figure 5 is 13.8-m long by 4.2-m diameter, with a 19.5-m solar-panel wingspan. With extensive use of graphite-epoxy structures, the mass is 4,800 kg.

The IUS performed two firings and then separated from the Observatory. After five firings of an internal propulsion system - the last of which took place 15 days after launch - the Observatory was placed in its highly elliptical orbit. This orbit has a nominal apogee of 140,000 km and a nominal perigee of 10,000 km. The inclination to the equator is 28.5^o. The satellite is above the radiation belts where the charged-particle background is so intense that no data may be taken for more than about 75% of the 63.5-hour orbital period. The observing efficiency, which also depends on solar activity, varies from 65% to more than 70%. Uninterrupted

Figure 3: Col. Eileen Collins.

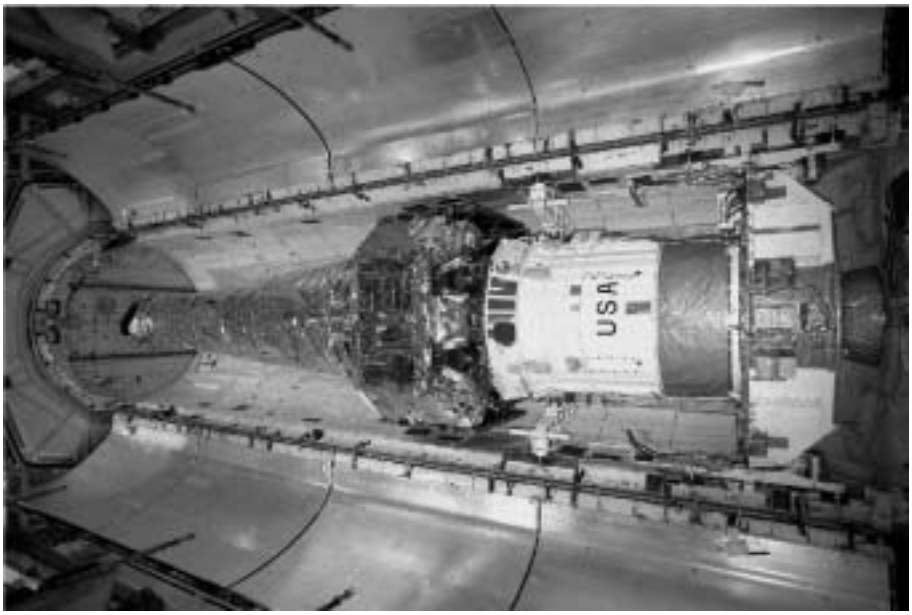

Figure 4: The Chandra X-Ray Observatory with the IUS attached and mounted in the cargo bay of the Space Shuttle Columbia.

Figure 5: Artist's drawing of the Chandra X-Ray Observatory with major components labeled.

observations lasting more than 2 days are thus possible.

The spacecraft itself has fairly unheroic capabilities except for its lightweight construction. The spacecraft provides pointing control, power, command and data management, thermal control, and other such services to the scientific payload. Electrical power is obtained from two 3-panel silicon solar arrays that provide over 2000 watts. Three 40-ampere-hour nickel-hydrogen batteries supply power during the rare eclipses. Two low-gain spiral antennas provide spherical communications coverage and the transmission frequency is 2250 MHz. The downlink provides selectable rates from 32 to 1024 kbps for communication with NASA's Deep Space Network (DSN) of ground stations. Commands are sent at a frequency 2071.8 MHz and the command rate is 2 kbps. Data are obtained from the instruments aboard the Observatory at a rate of 24 kbs and are recorded using a solid-state recorder with 1.8 gigabits (16.8 hours) of recording capacity. Instrument data, together with 8 kbs of spacecraft data primarily from the aspect camera system, are downloaded to the DSN typically every 8 hours. The ground stations then transmit the information to the Chandra Science Center in Cambridge MA where the operations control is performed. The Observatory is designed to operate autonomously, if necessary, for up to 72 hours and no ground intervention is required to place the Observatory in a safe configuration after any single fault is detected.

Attitude and momentum control utilizes 6 reaction wheels and liquid fuel thrusters. Two inertial reference units, each with two redundant two-degree-of-freedom gyroscopes are updated automatically with data from an aspect camera. Control of the spacecraft momentum is required both for maneuvers and to maintain stable attitude during observations. Momentum control is accomplished using the 6 reaction wheels which are mounted in a pyramidal configuration. During observing, with the spacecraft attitude constant, apart from a dither pattern introduced to spread the image out over many focal-plane detector pixels, external torques on the spacecraft will cause a buildup of angular momentum. This momentum is then shed by firing small thrusters and simultaneously spinning down the reaction wheels. The pointing stability is 0.25 arcsec (RMS) radius over 95% of all 10-second periods and the pointing accuracy is better than 30 arcsec.

The principal elements of the payload are the aspect system used to determine where the observatory was pointed, the x-ray telescope, and the scientific instruments. The specified design life of the mission is 5 years; however, the only

perishable (gas for maneuvering) is sized to allow operation for more than 10 years. The orbit will be stable for decades. The life of the Observatory is thus limited by the reliability of the component parts.

2 The Aspect Camera

The aspect camera system includes a 11.2-cm, F/9, Ritchey-Chretien, visible-light telescope and CCD camera attached to the x-ray telescope. The detector is a 1024×1024 Tektronix CCD, with 24×24 micron (5×5 arcsec) pixels, covering the band between 4000 and 9000 Å. The system field-of-view is 1.4×1.4 deg. The CCD is placed out of focus to spread the star image over several pixels to increase the accuracy of the centering algorithm.

Surrounding each of the x-ray focal plane detectors is a set of fiducial light emitting diodes. Each fiducial light produces a collimated beam at 635 nm which is imaged onto the aspect camera's CDD using a periscope and transfer mirror. The images of the fiducial lights are used to determine the instrument position relative to the x-ray telescope axis and the stars imaged by the aspect camera. The aspect solution's accuracy depends on the number of stars detected in the field, but is typically 0.6 seconds of arc.

A sun-shade (also shown in Figure 6) protects the camera from the light from the Sun, Earth and Moon, with avoidance angles of 45^o, 20^o and 6^o, respectively. Only light from the sun can damage the system, the other objects in the field-of view would only saturate the detector output without damage and therefore only limit the aspects camera's utility during observations. The Moon (Figure 7) has been viewed with the Observatory, in part to study the background signal, and in part to learn about the Moon's chemical composition.

3 The X-Ray Optics

The heart of the Observatory is the x-ray telescope made of four concentric, precision-figured, superpolished Wolter-1 telescopes, similar to those used for both the Einstein and Rosat observatories, but of much higher quality, larger diameter, and longer focal length. Each individual element is 83.3 cm long, constructed of Zerodur material, and polished to better than a few angstroms root-mean-square

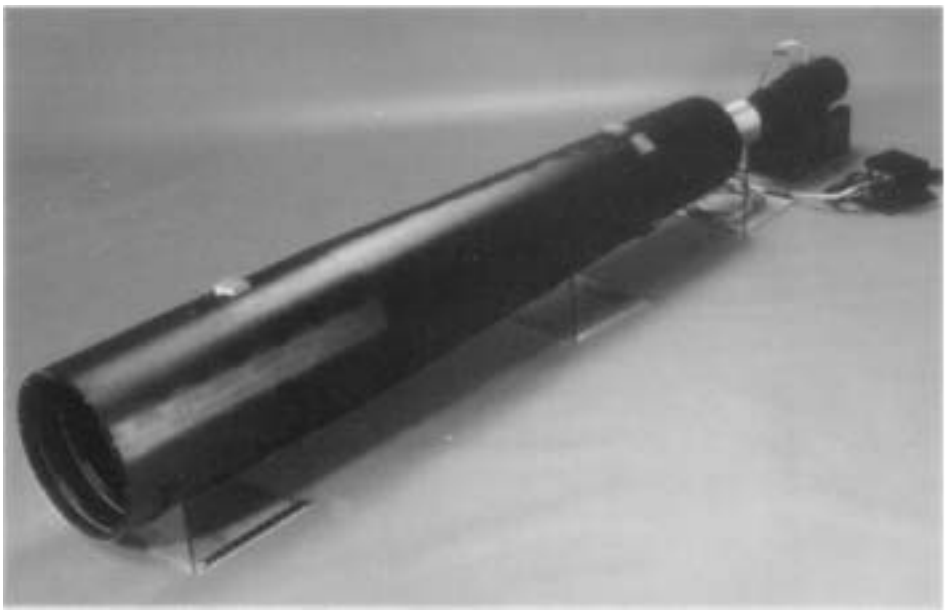

Figure 6: Photograph of the aspect camera with sunshade.

Figure 7: Optical and X-Ray images of the Moon. Optical: Courtesy Robert Gendler; X-ray: NASA/CXC/SAO/J.Drake et al.[1]

(RMS) microrougness. Zerodur, a glassy ceramic, was chosen for its high thermal stability. The Set of 8 mirrors weighs 956 kg. The focal Length is 10 meters, the outer diameter is 1.2 meters, the field of view is 1 degree (FWHM) in diameter and the clear aperture is 1136 cm^2.

The Wolter-1 design uses a paraboloid of revolution followed by a hyperboloid of revolution. Two reflections minimize coma. The mirrors are coated with 600 angstroms of iridium, chosen for high reflectivity at the x-ray energies of interest, 0.08 - 10.0-keV (15-0.12 nm).

3.1 Point Spread Function

The telescope's point spread function, as measured during ground calibration, had a full width at half-maximum less than 0.5 arcsec and a half-power diameter less than 1 arcsec. The pre-launch prediction for the on-orbit encircled-energy fraction was that a 1-arcsec-diameter circle would enclose at least half the flux from a point source. A relatively mild dependence on energy, resulting from diffractive scattering by surface microroughness, attests to the 3-angstroms-rms surface roughness. The ground measurements were taken under environmental conditions quite different than those encountered on-orbit. The effects of gravity, the finite source distance, and the size of the various x-ray sources used to calibrate the observatory at a specially constructed test facility at NASA's Marshall Space Flight Center (Figure 8) were unique to the ground calibration. On-orbit the performance includes the spatial resolution of the flight detectors and uncertainties in the aspect solution. The on-orbit performance met expectations as illustrated in Figure 9.

The tremendous advancement in angular resolution, almost a factor of 10, that the Chandra optics provides, introduces new considerations for the analysis of the data. For example, one now has to account for the energy dependence of the flux scattered out of the beam by the interstellar medium.

4 Instrumentation

The instrument module includes mechanisms for focusing and translating the imaging detectors into position at the focus of the telescope. Positioning of the instruments is required as x-ray beam-splitters are not very efficient. In addition

Figure 8: Aerial view of the X-Ray Calibration Facility at NASA's Marshall Space Flight Center. The large building to the right houses a thermal-vacuum chamber. A 525-m evacuated tube connects the chamber to various X-ray sources.

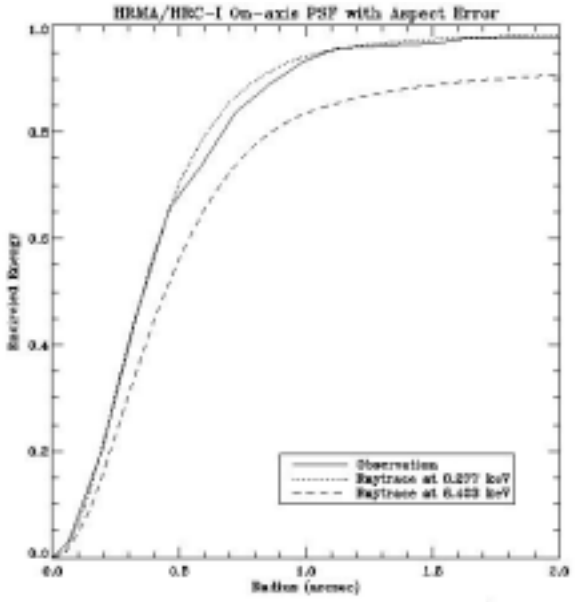

Figure 9: Encircled energy versus radius comparing pre-launch predictions at two energies to on-orbit performance.

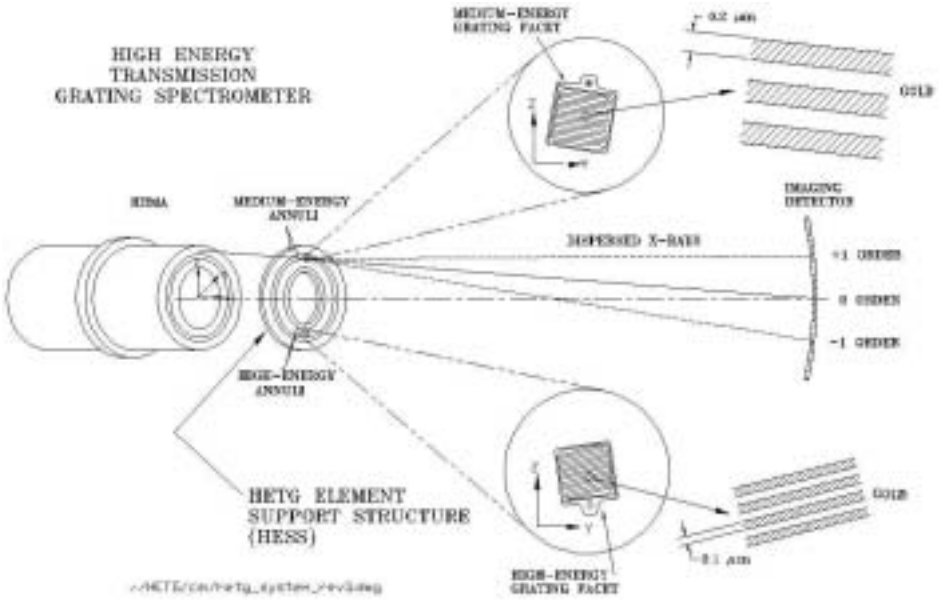

Figure 10: HETGS layout and principle of operation.

to the imaging detectors there are two transmission gratings. These are placed just behind the telescope and are the Low-Energy Transmission Grating (LETG), optimized for longer x-ray wavelengths and the High-Energy Transmission Grating (HETG), optimized for shorter wavelengths. The gratings allow for measurements with spectral resolving power of $E/\delta\ E > 500$ for wavelengths of > 0.4-nm (energies < 3 keV). Positioning mechanisms are used to insert either (but not both!) grating arrays into the converging beam to disperse the x-radiation onto the focal plane producing high-resolution spectra read-out by one of the imaging detectors. Figure 10 illustrates the concept for the HETG. The LETG is similar except in concept but all the facets are identical.

The Space Research Institute of the Netherlands and the Max-Planck-Institüt für Extraterrestrische Physik designed and fabricated the LETG. The assembly is made of 540 grating facets with gold bars of 991-nm period. The LETG provides high-resolution spectroscopy from 0.08 to 2 keV (15 to 0.6 nm). The Massachusetts Institute of Technology (MIT) designed and fabricated the HETG. The HETG uses 2 types of grating facets - the Medium-Energy Gratings (MEG) which, when inserted, are placed behind the telescope's 2 outermost shells, and the High-Energy

Gratings (HEG), behind the 2 innermost shells. The HEG and MEG are oriented at slightly different dispersion directions in order to easily distinguish the images of the dispersed spectra. With polyimide-supported gold bars of 400-nm and 200-nm periods, the HETG provides high-resolution spectroscopy from 0.4 to 4 keV (MEG, 3 to 0.3 nm) and from 0.8 to 8 keV (HEG, 1.5 to 0.15 nm).

Chandra's two focal-plane science instruments are the High Resolution Camera (HRC) and the Advanced CCD Imaging Spectrometer (ACIS). SAO designed and fabricated the HRC. One of the HRC detectors is made of a 10-cm-square microchannel plate, and provides high-resolution imaging over a 31-arcmin-square field of view. A second detector, comprising 3 rectangular segments (3-cm-by-10-cm each) mounted end-to-end along the grating dispersion direction, serves as the primary read-out detector for the LETG. Both of the HRC detectors are coated with a cesium-iodide photocathode and have thin aluminized polyimide shields to prevent contamination by ions and ultraviolet light.

The Pennsylvania State University and MIT built the Advanced CCD Imaging System (ACIS) with charge-coupled devices (CCDs) fabricated by MIT's Lincoln Laboratory. As with the HRC, there are two detector systems. One is made of a 2-by-2 array of CCDs, and provides high-resolution spectrometric imaging over a 17-arcmin-square field of view. The other, a 6-by-1 array mounted along the grating dispersion direction, serves as the primary read-out detector for the HETG. The ACIS uses two types of CCDs, 8 front-illuminated (FI) and two back-illuminated (BI). The BI CCDs have higher efficiency at lower energies than the FI devices, but were much more difficult to fabricate. One BI CCD was placed at the on-axis focal position of the 6 x 1 array. Thus, this particular CCD also provides high-resolution spectrometric imaging extending to lower energies, but over a smaller (8-arcmin-square) field than the 2 x 2 array. The other BI device is also in the 6 x 1 array. Both ACIS detector systems have thin aluminized polyimide filters to minimize contamination by visible light.

Despite successful science operations, the Observatory has had to deal with a number of technical difficulties that have had their impact on scientific performance. The front- (not the back-) illuminated ACIS CCDs suffered damage, which increased the charge transfer inefficiency, and hence the energy resolution, as a result of bombardment by low-energy (100 keV) protons crudely focused by the telescope by means of Rutherford scattering as the Observatory entered the radiation belts. Following a procedure of removing ACIS from the focal plane

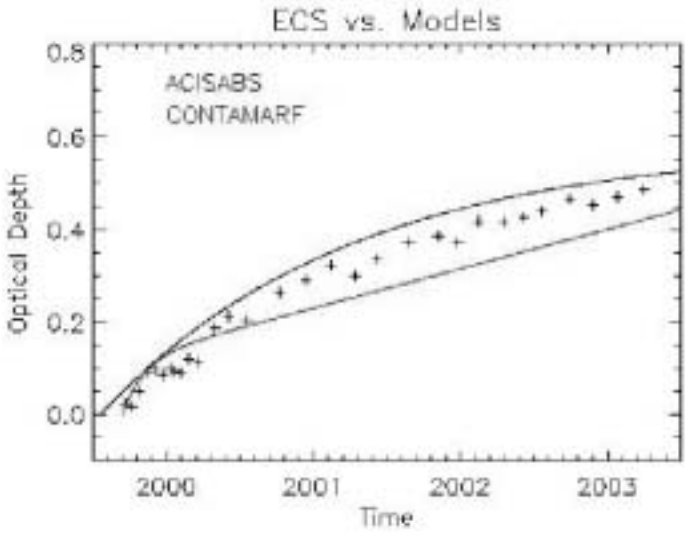

Figure 11: Optical depth at the carbon edge of the ACIS filters versus time compared with two different contamination models.

during radiation belt passages has dramatically minimized subsequent increases in the charge transfer inefficiency. O'Dell et al.[2] discuss the Chandra approach to radiation management.

Both ACIS filters are among the coldest (120-C) surfaces on the observatory and are collecting hydrocarbon contamination at the rate of about one-half an optical depth at the Carbon K-edge per year. Figure 11 illustrates the contamination build up based on two different methods of quantifying the impact and our current understanding of the chemical composition and rate of deposition of the contaminants. Marshall et al.[3] discuss the composition of the contaminant. Normally, one would plan to bake off the contamination. Bakeout is, however, complicated by the potential negative impact on the charge transfer efficiency of the CCDs. A bakeout strategy that involves a minimum temperature increase is being developed.

5 Useage

The CXC has recently completed the review of proposals in response to the fifth announcement of opportunity - the first was issued a year before launch. There were 785 proposals with Principal Investigators from 21 countries. These proposals included 14 Very Large Projects (defined as those that require more than 1000 ksec to perform), 54 Large Projects (those that require 300 ksec or more), 71 proposals to use the Chandra archives, and 40 proposals to perform theoretical research that has direct impact on the analysis and interpretation of Chandra data. The peer review accepted 208 observing proposals of which 3 were very large projects, 7 were large projects. In addition, 17 archive and 18 theory proposals were accepted.

6 Discoveries

The first X-rays focused by the telescope were observed on August 12, 1999. Figure 12 shows one of the early images. This image of the Crab Nebula and its pulsar included a major new discovery - the bright inner elliptical ring showing the first direct observation of the shock front where the wind of particles from the pulsar begins to radiate in X-rays via the synchrotron process. Discoveries of new astronomical features in Chandra images have been the rule, not the exception.

The Observatory's capability for high-resolution imaging enables detailed high-resolution studies of the structure of extended x-ray sources, including supernova remnants, astrophysical jets, and hot gas in galaxies and clusters of galaxies. Equally important are Chandra's unique contributions to high-resolution dispersive spectroscopy. As the capability for visible-light spectroscopy initiated the field of astrophysics about a century ago, high-resolution x-ray spectroscopy now contributes profoundly to the understanding of the physical processes in cosmic x-ray sources and is the essential tool for diagnosing conditions in hot plasmas. The high spectral resolution of the Chandra gratings isolates individual lines from the myriad of spectral lines, which would overlap at lower resolution. The additional capability for spectrometric imaging allows studies of structure, not only in x-ray intensity, but also in temperature and in chemical composition. Through these observations, users are addressing several of the most exciting topics in contemporary astrophysics.

In addition to mapping the structure of extended sources, the high angular

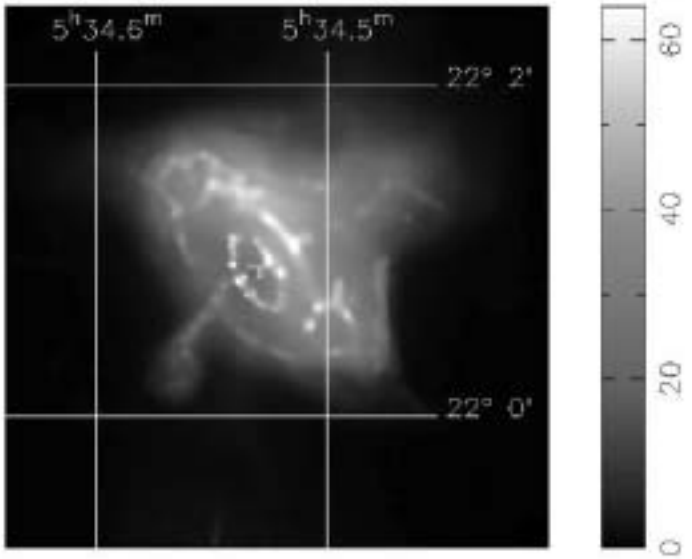

Figure 12: Adaptively smoothed image of the Crab Nebula.

resolution permits studies of discrete sources, which would otherwise be impossible. An example is shown in Figure 13 where one sees X-rays produced by TWA 5B, a brown dwarf orbiting a young binary star system known as TWA 5A6. This observation is important not only for demonstrating the importnace of angular resolution but for addressing the question as to how do brown dwarfs heat their upper atmospheres (coronas) to x-ray-emitting temperatures of a few million degrees.

From planetary systems to deep surveys of the faintest and most distant objects, the scientific results from the first four years of Chandra operations have been exciting and outstanding. We conclude this overview with a series of images illustrating some of these results.

We begin with images of the x-ray emission from the planet Jupiter. Figure 14 shows hot spots at high (and unexpected) latitudes that appear to pulsate at approximately a 45-minute period.[4] In this case the X-rays appear to be produced by particles bombarding the Jovian atmosphere after precipitating along magnetic field lines. Figure 15 continues the discoveries about the Jovian system and shows the first detection of X-rays from two of the moons – Io and Europa.[5]

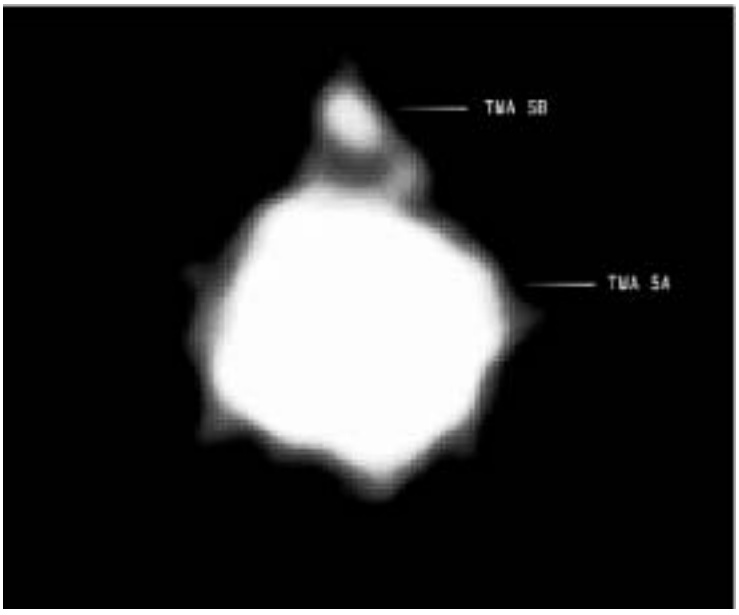

Figure 13: X-rays produced by TWA 5B, a brown dwarf orbiting a young binary star system known as TWA 5A. The image is 6-arcsec on a side. Courtesy of NASA/CXC/Chuo U.

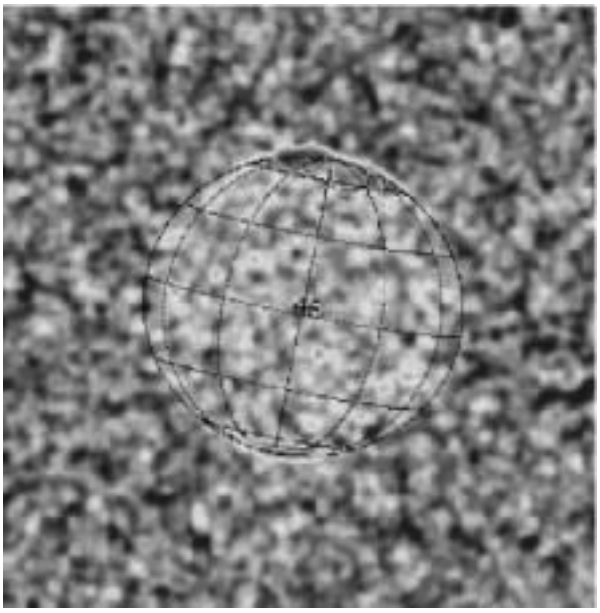

Figure 14: Chandra image of Jupiter showing the hot spots at high latitudes. The image is 50–arcsec on a side. Courtesy R. Elsner.

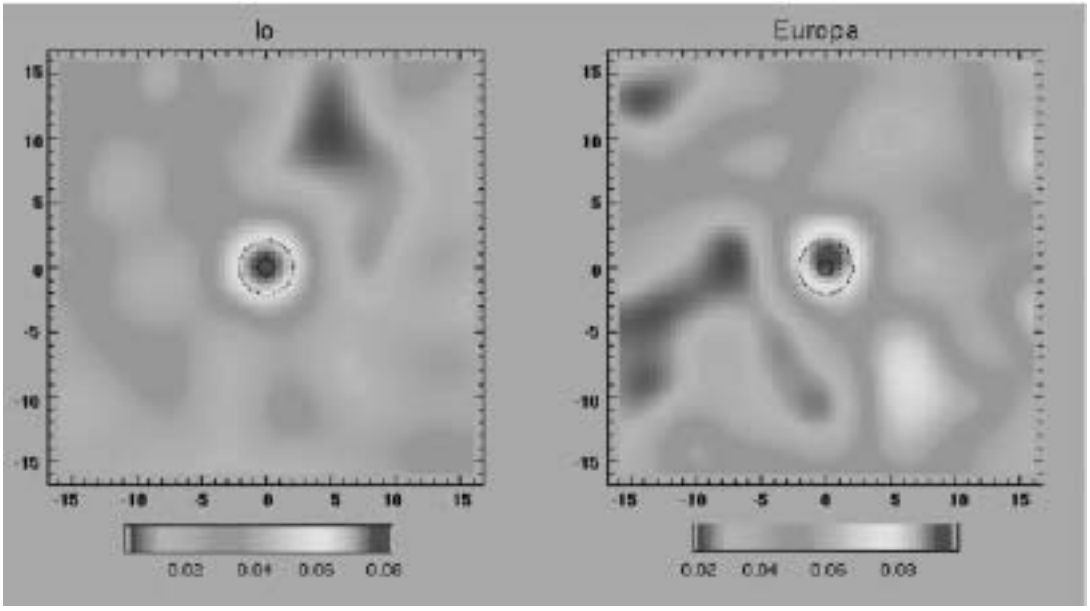

Figure 15: Chandra images of the Jovian moons Io and Europa. Courtesy R. Elsner.

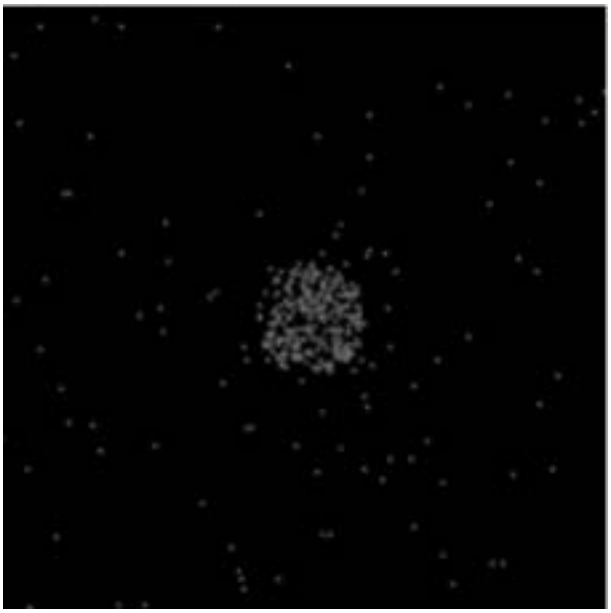

Figure 16: Chandra image of Mars. Image is 2 arcmin on a side and the Mars disk is 20.3 arcsec in diameter. Courtesy NASA/CXC/MPE/K.Dennerl.

In Figure 16 we show the more recent detection[6] of fluorescent scattering of solar X-rays in the upper atmosphere of Mars. The x-ray spectrum is dominated by a single narrow emission line, which is most likely caused by oxygen K-shell fluorescence.

One of the most spectacular Chandra images is the one of the center of our own galaxy[7] shown in Figure 17. Here we clearly see both point-like discrete sources (over 1000) and diffuse extended emission. This large amount of hot x-ray emitting gas has been heated and chemically enriched by numerous stellar explosions.

Figure 18 shows a time history and relative positioning of the optical emission of SNR 1987A as seen with the Hubble Space Telescope (HST) together with the x-ray emission observed with Chandra.[8] The reverse, x-ray emitting, shock, inside of the cooler, optically-emitting, gas is a textbook example of the shock-heating of the interstellar medium following the stellar explosion.

The final legacy of Chandra may ultimately be led by the spectroscopic data. The energy resolution, enabled by the quality of the optics, is providing new

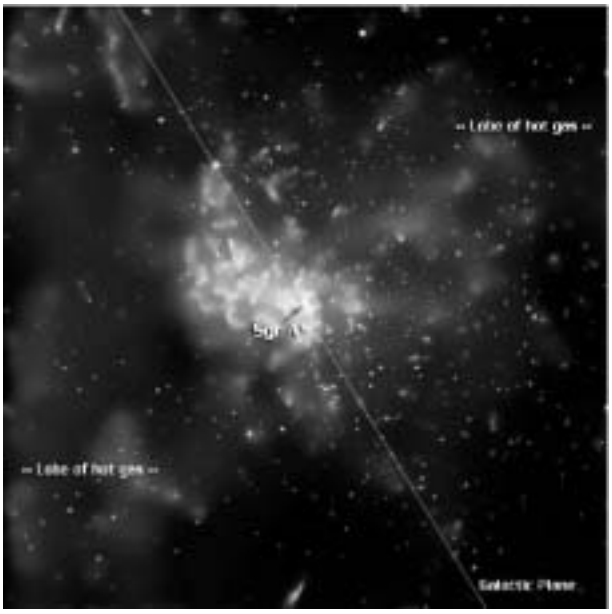

Figure 17: Chandra image of the Galactic Center. The image is 8.4 arcmin on a side. Courtesy NASA/CXC/MIT/F.K.Baganoff et al.

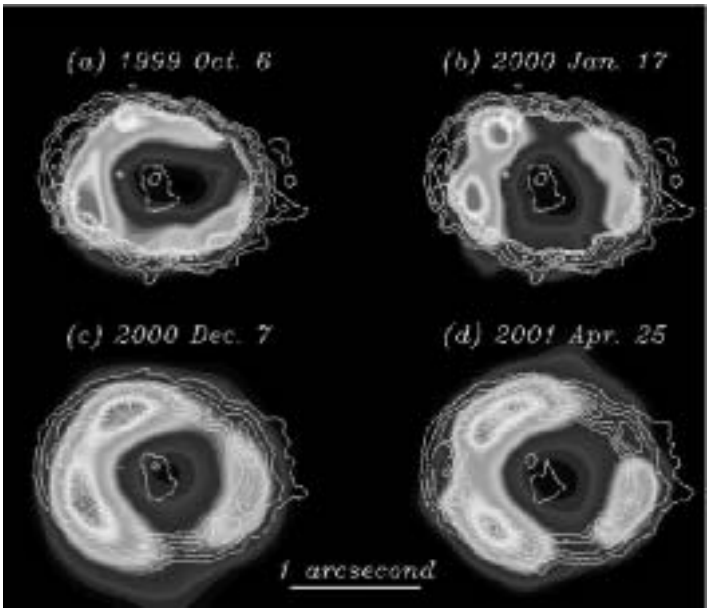

Figure 18: ACIS images and HST contours of the emission from SNR1987A. Courtesy Dave Burrows.

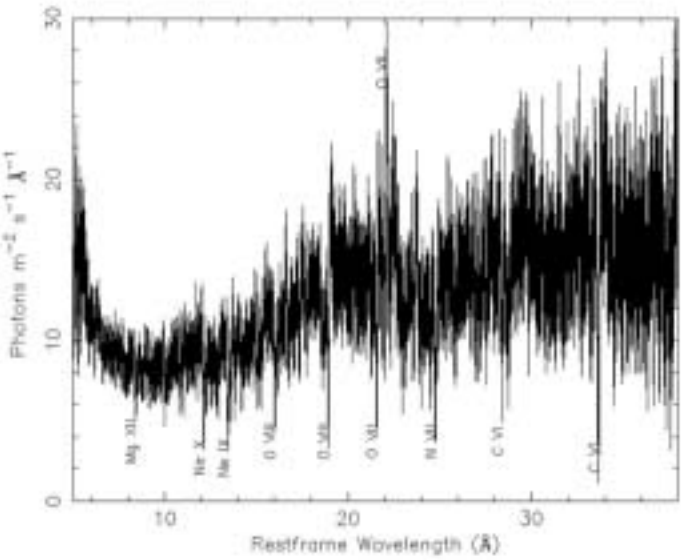

Figure 19: LETG/HRC spectrum of the Seyfert 1 galaxy NGC 5548.[9] Several prominent absorption lines from H-like and He-like ions are marked, as is the forbidden line of He-like oxygen.

and extremely complex results. For example, high-resolution spectra of Seyfert galaxies are providing new details about the physical and dynamical properties of material surrounding the active nucleus. In the case of Seyfert-1s, whose signal is dominated by a bright x-ray continuum from the central engine, the partially ionized circum-source material introduces prominent patterns of absorption lines and edges. Figure 19, e.g. shows a LETG/HRC spectrum of NGC 5548. This spectrum has dozens of absorption lines.[9] For Seyfert 2's the strong continuum from the central engine is not seen directly, so the surrounding regions are seen in emission. Figure 20 provides an example of a LETG/HRC observation of NGC 1068.[10]

One of the more important triumphs of the Observatory has been to use the angular resolution and high sensitivity to perform detailed surveys of extended objects such as globular clusters, galaxies, and clusters of galaxies. Figure 21 shows one of the spectacular Chandra images of globular clusters.[11] A survey of two interacting galaxies is illustrated in Figure 22 where one sees emission from

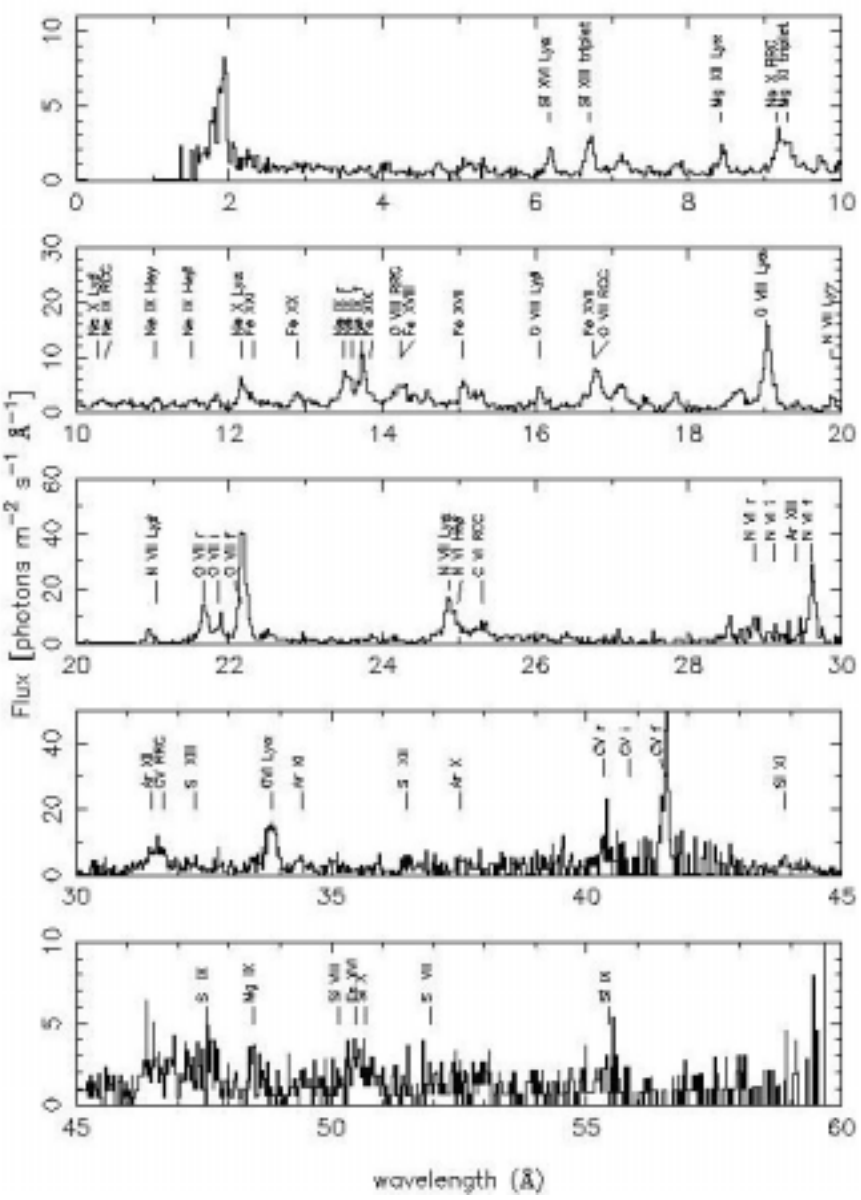

Figure 20: Emission-line spectrum from the Seyfert 2 galaxy NGC 1068. Kindly provided by A. Kinkhabwala.

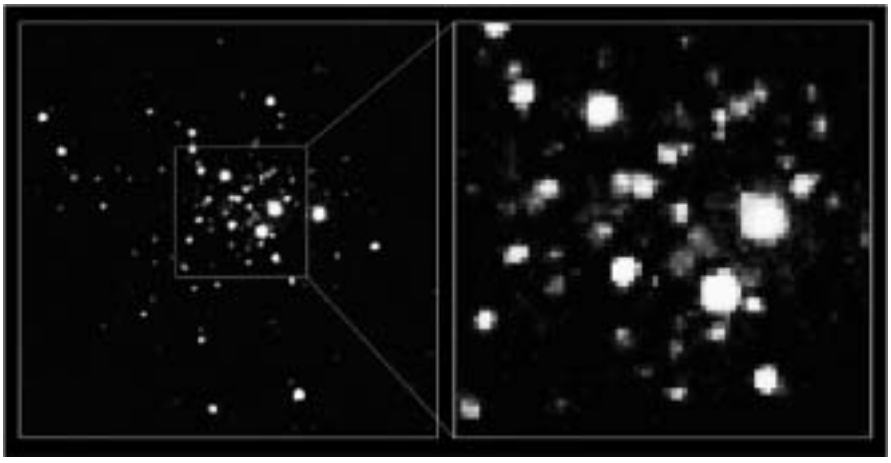

Figure 21: Chandra ACIS image of the globular cluster 47 Tucanae. The left panel covers the central 2' x 2.5'. The central 35" x 35" are shown to the right. Courtesy NASA/CfA/J.Grindlay et al.

diffuse gas and bright point sources.

Chandra observations of clusters of galaxies frequently exhibit previously undetected structures with characteristic angular scales as small as a few arc seconds. These include "bubbles" where there is strong radio emission, bow shocks, and cold fronts. These phenomena are illustrated in the sequence of figures, 23-25. Figure 23 of the Perseus cluster[12] is a spectacular example of bubbles produced in regions where there is strong radio emission. Figure 24 shows a bow shock propagating in front of a bullet-like gas cloud just exiting the disrupted cluster core. This observation provided the first clear example of such a shock front.[13] In contrast, Figure 25 of Abell 2142[14] shows an example of a shockless cold front.

A major triumph of Chandra (and XMM-Newton) high-resolution spectroscopic observations has been the discovery that that gas in the clusters is typically *not* cooling to below about 1-2 keV[15] which indicates the presence of one (or more) heating mechanisms.

Some clusters, such as Abell 2029 shown in Figure 26, do exhibit a smoother relaxed structure. Here we see the thousands of galaxies inside the cocoon of hot, x-ray-emitting gas. Measurement of the temperature and density profiles of the gas, inwards towards the central, dominant galaxy, provides a map of the

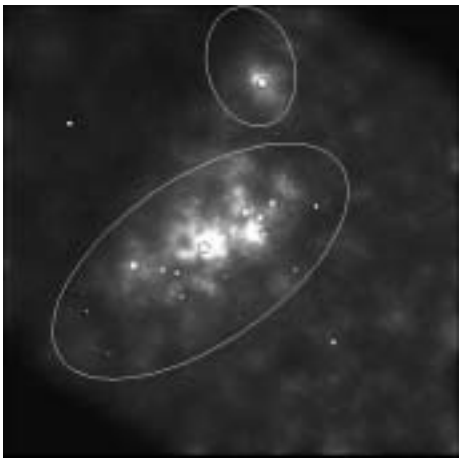

Figure 22: X-ray image of two interacting galaxies NGC 4490 and 4485. The image is 8-arcmin on a side. Large ovals represent the approximate boundaries of the galaxies (NGC 4490 is the larger of the two). Small circles indicate the brightest X-ray sources. Courtesy Doug Swartz.

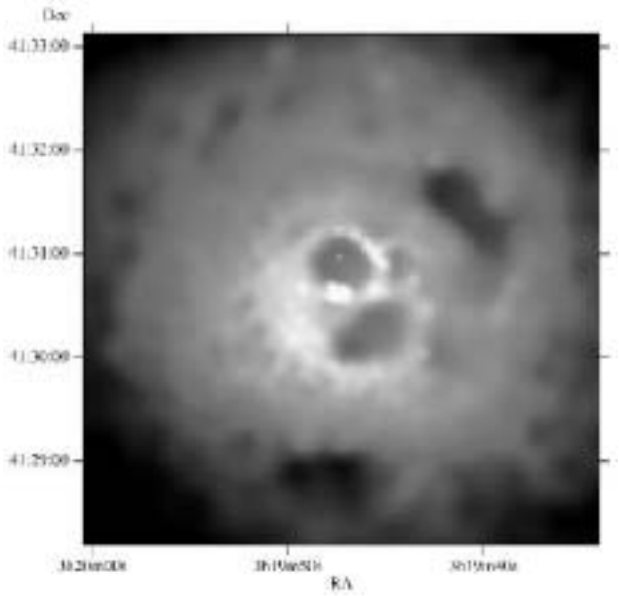

Figure 23: X-ray core of the Perseus cluster. The image is about 3.5 arcmin on a side. Courtesy NASA/IoA/A. Fabian et al.

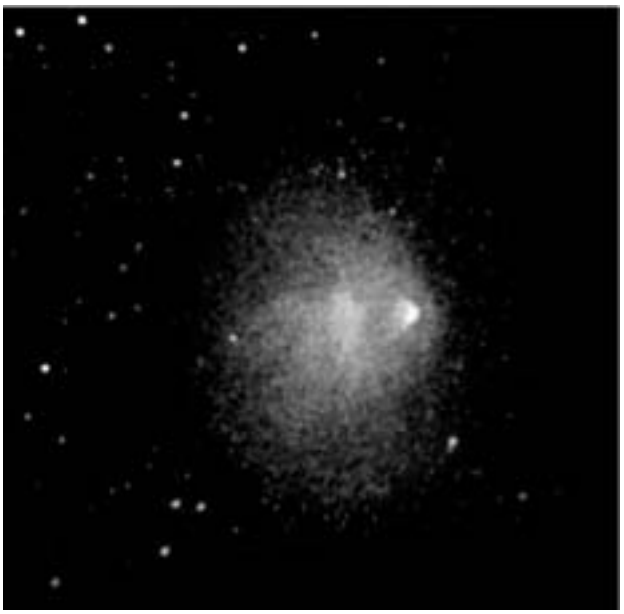

Figure 24: The Chandra image of the merging, hot galaxy cluster 1E 0657-56. The image is about 9 arcmin on a side. Courtesy NASA/SAO/CXC/M.Markevitch et al.

Figure 25: Chandra Image of the galaxy cluster Abell 2142. The image is 8.4 arcmin on a side. The sharp border to the top right is an example of a cold front. Courtesy NASA/CXC/SAO

gravitational potential, and hence the dark matter in the cluster. The observers, Lewis, Buote, and Stocke,[16] showed that the dark matter density increased toward the center in a manner consistent with cold dark matter models.

The study of active galaxies is one of the centerpieces of studies with the Observatory. Figure 27 illustrates a recent spectacular result — the first image of a double quasar nucleus.[17]

Figure 28 illustrates multiwavelength observations of the jets from active galaxies. The Chandra x-ray image[18] shows an irregular, knotty structure similar to that seen at radio and optical[19] wavelengths. However, the knots near the central core are much brighter in X-rays

The jet phenomenon now appears to be ubiquitous in astronomical settings, especially with regards to x-ray emission. One of the most interesting recent Chandra discoveries has been the series of observations of the outer jet of the Vela pulsar[20] a few of which are illustrated in Figure 29 where we see the jet, always confined to a narrow segment, but moving about at velocities of about 0.3-0.5 c.

No discussion of data taken with the Observatory is complete without a mention of the deep surveys. These are deep exposures of particular regions of the

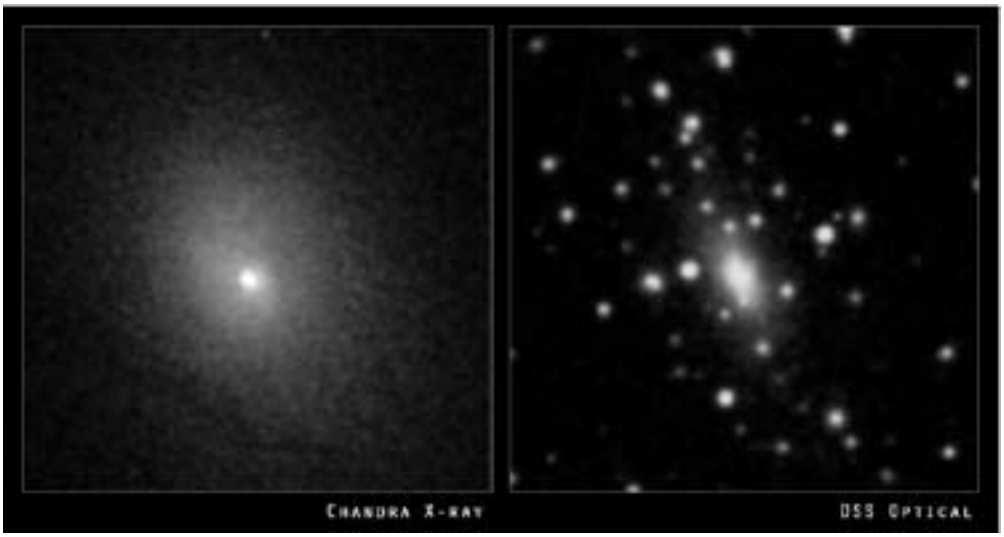

Figure 26: X-ray (left) and optical (right) images of the galaxy cluster Abell 2029. The images are 4-arcmin on a side. X-ray: NASA/CXC/UCI/A. Lewis et al. Optical: Pal.Obs. DSS

sky to study the populations of the objects detected, especially the faintest ones. This work is an outgrowth of the study the diffuse x-ray background, the nature of which had been a puzzle for nearly 40 years, although the lack of distortion of the spectrum of the Cosmic Microwave Background placed a strong upper limit to the possibility of a truly diffuse component.[21] Observations with ROSAT at energies below 2 keV made a major step in resolving a significant fraction (70-80%) into discrete objects.[22] Currently two long exposures have been accomplished with the Chandra X-Ray Observatory - the Chandra Deep Field North[23] depicted in Figure 30 with 2-Ms of exposure, and the Chandra deep field south[24] with 1-Msec. These surveys have extended the study of the background to flux levels more than an order of magnitude fainter than previously in the 0.5-2.0 keV band and have resolved over 90% of the background into a variety of discrete sources. The largest uncertainty in establishing the fraction is now in the knowledge of the total level of the background itself.

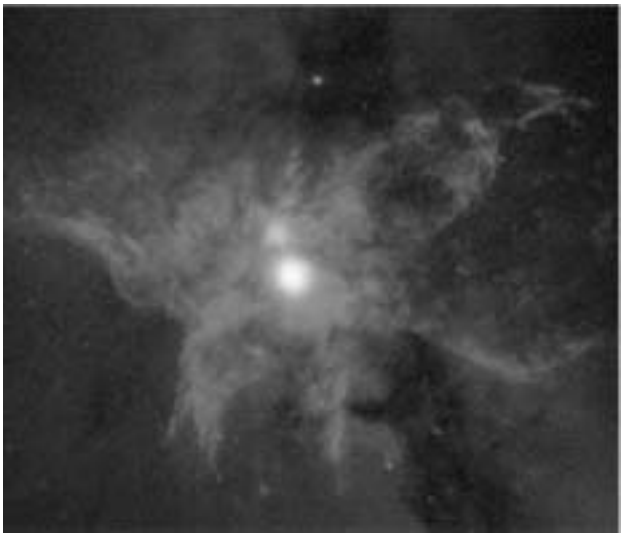

Figure 27: The Chandra image of NGC 6240, a butterfly-shaped galaxy that is the product of the collision of two smaller galaxies, shows that the central region contains two active galactic nuclei. The image is 0.35 x 0.3 arcmin. Courtesy NASA/CXC/MPE/S.Komossa et al.

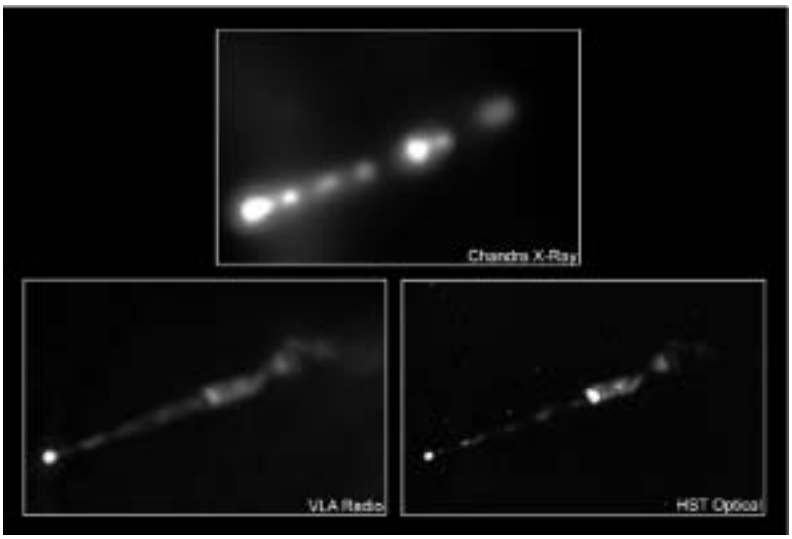

Figure 28: The x-ray jet emanating from the nucleus of the elliptical galaxy M87 as seen in three wavelength bands. Credits: X-ray: NASA/CXC/MIT/H. Marshall et al. Radio: F. Zhou, F.Owen (NRAO), J.Biretta (STScI) Optical: NASA/STScI/UMBC/E.Perlman et al.

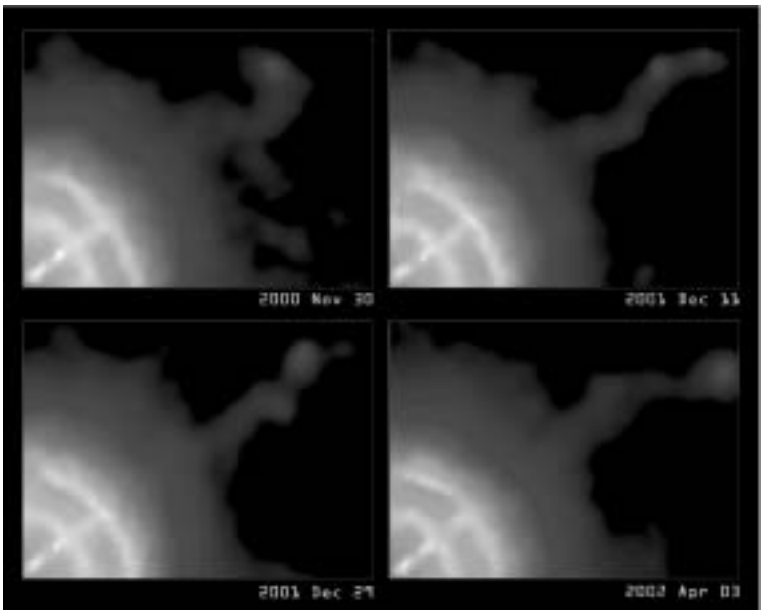

Figure 29: Four observations of the Vela Pulsar and its outer jet. Each image is 1.6 x 1.2 arcmin Courtesy NASA/CXC/PSU/G. Pavlov et al.

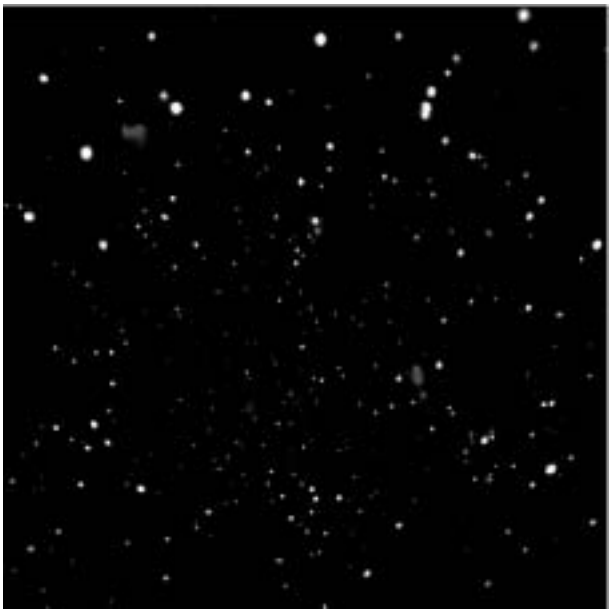

Figure 30: Two-million-second image of the Chandra Deep Field North. Courtesy NASA/CXC/PSU/D.M. Alexander, F.E. Bauer, W.N. Brandt et al.

7 WORLD-WIDE WEB SITES

The following lists several Chandra-related sites on the World-Wide Web:

http://chandra.harvard.edu/: Chandra X-Ray Center (CXC), operated for NASA by the Smithsonian Astrophysical Observatory.

http://wwwastro.msfc.nasa.gov/xray/axafps.html: Chandra Project Science, at the NASA Marshall Space Flight Center.

http://hea-www.harvard.edu/HRC/: Chandra High-Resolution Camera (HRC) team, at the Smithsonian Astrophysical Observatory (SAO).

http://www.astro.psu.edu/xray/axaf/axaf.html: Advanced CCD Imaging Spectrometer (ACIS) team at the Pennsylvania State University (PSU).

http://acis.mit.edu/: Advanced CCD Imaging Spectrometer (ACIS) team at the Massachusetts Institute of Technology.

http://www.sron.nl/missions/Chandra: Chandra Low-Energy Transmission Grating (LETG) team at the Space Research Institute of the Netherlands.

http://wave.xray.mpe.mpg.de/axaf/: Chandra Low-Energy Transmission Grating (LETG) team at the Max-Planck Institüt für extraterrestrische Physik (MPE).

http://space.mit.edu/HETG/: Chandra High-Energy Transmission Grating (HETG) team, at the Massachusetts Institute of Technology

http://hea-www.harvard.edu/MST/: Chandra Mission Support Team (MST), at the Smithsonian Astrophysical Observatory.

http://ifkki.kernphysik.uni-kiel.de/soho: EPHIN particle detector.

References

[1] Pictures that are publicly available at the Chandra web site at http://chandra.harvard.edu have credits labeled "Courtesy ... NASA/". The acronyms may be found at this site.

[2] O'Dell, Stephen L., Blackwell, William C., Jr., Cameron, Robert A., Minow, Joseph I., Morris, David C., Spitbart, Bradley J., Swartz, Douglas A., Virani, Shanil N., Wolk, Scott J. 2003, SPIE, **4851**, 77.

[3] Marshall, H., Tennant, A., Grant, C.E., Hitchcock, A.P., O'Dell, S.L., & Plucinsky, P.P. 2003, SPIE, **5165**.

[4] Gladstone, R. et al. 2002, Nature, **415**, pp. 1000-1003.

[5] Elsner, R. F. et al. 2002, The Astrophysical Journal, **572**, pp 1077-1082.

[6] Dennerl, K. 2002, A&A, **394**, 1119.

[7] Baganoff, F.K., Maeda, Y., Morris, M., Bautz, M.W., Brandt, W.N., Cui, W., Doty, J.P., Feigelson, E.D., Garmire, G P., Pravdo, S.H., Ricker, G.R.,& Townsley, L.K. 2003, The Astrophysical Journal,**591**, pp. 891-915.

[8] Burrows, D. et al. 2000, The Astrophysical Journal, **543**, L149.

[9] Kaastra, J.S., Mewe, R., Liedahl, D.A., Komossa, S., & Brinkman, A.C. 2000, Astronomy and Astrophysics, **354**, L83.

[10] Brinkman, A.C., Kaastra, J. S., van der Meer, R.L.J., Kinkhabwala, A., Behar, E., Paerels, F., Kahn, S.M. & Sako, M. 2002, Astronomy and Astrophysics, **396**, pp.761-772.

[11] Grindlay, J. E., Heinke, C., Edmonds, P. D., & Murray, S. S. 2001, Science, **290**, p. 2292.

[12] Fabian, A.C., Sanders, J.S., Ettori, S., Taylor, G.B., Allen, S.W., Crawford, C.S., Iwasawa, K., Johnstone, R.M., & Ogle, P.M. 2000, MNRAS, **318**, L65.

[13] Markevitch, M., Gonzalez, A.H., David, L., Vikhlinin, A., Murray, S., Forman, W., Jones, C., Tucker, W. 2002, The Astrophysical Journal, **567**, pp. L27-L31.

[14] Markevitch, M., Ponman, T.J., Nulsen, P.E.J., Bautz, M.W., Burke, D.J., David, L.P., Davis, D., Donnelly, R.H., Forman, W.R., Jones, C., & 12 coauthors, 2000, The Astrophysical Journal, **541**, pp. 542-549.

[15] See for example the discussion in Fabian, A.C. 2002, "Cooling Flows in Clusters of Galaxies" in Lighthouses of the Universe: The Most Luminous Celestial Objects and Their Use for Cosmology, Proceedings of the MPA/ESO/, p. 24.

[16] Lewis, A.D., Buote, D.A., & Stocke J.T. 2003, Astrophysical Journal, **586**, pp. 135-142.

[17] Komossa, S., Burwitz, V., Hasinger, G., Predehl, P., Kaastra, J. S., & Ikebe, Y. 2003, The Astrophysical Journal, **582**, pp. L15-L19.

[18] Marshall, H.L., Miller, B.P., Davis, D.S., Perlman, E.S., Wise, M., Canizares, C.R., & Harris, D.E. 2002, The Astrophysical Journal, **564**, pp. 683-687.22

[19] Perlman, E. S. et al. 2001, The Astrophysical Journal, **561**, pp. L51-L54.

[20] Pavlov, G. G., Teter, M. A., Kargaltsev, O., & Sanwal, D. 2003, The Astrophysical Journal, **591**, pp. 1157-1171.

[21] Mather, J. C. et al. 1990, The Astrophysical Journal, **354**, L4. See also Prof. Kahn's two lectures.

[22] Hasinger, G. et al. 1998, Astronomy and Astrophysics, **329**, 482.

[23] Alexander, D. M., Bauer, F. E., Brandt, W. N., Hornschemeier, A. E., Vignali, C., Garmire, G. P., Schneider, D. P., Chartas, G., & Gallagher, S. C. 2003, The Astronomical Journal, **125**, pp. 383-397. and references therein.

[24] Giacconi, R., Rosati, P., Tozzi, P., Nonino, M., Hasinger, G., Norman, C., Bergeron, J., Borgani, S., Gilli, R., Gilmozzi, R., & Zheng, W. 2001, Astrophysical Journal, **551**, p. 642.